Article

Optical and structural characterization of a chronic myeloid leukemia DNA biosensor

Milton Cordeiro, Ana Rita Otrelo-Cardoso, Dmitri I. Svergun, Petr V. Konarev, João Carlos Lima, Teresa Santos-Silva, and Pedro Viana Baptista

ACS Chem. Biol., **Just Accepted Manuscript** • DOI: 10.1021/acschembio.8b00029 • Publication Date (Web): 21 Mar 2018

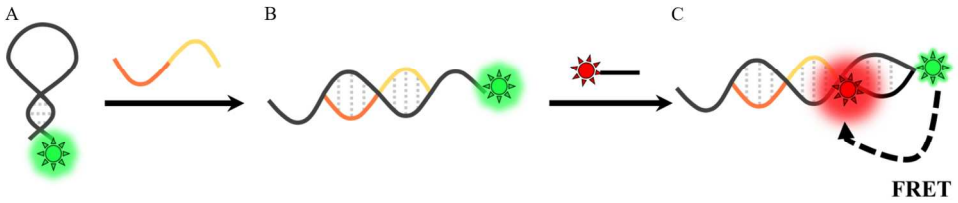

Figure 1

535x117mm (96 x 96 DPI)

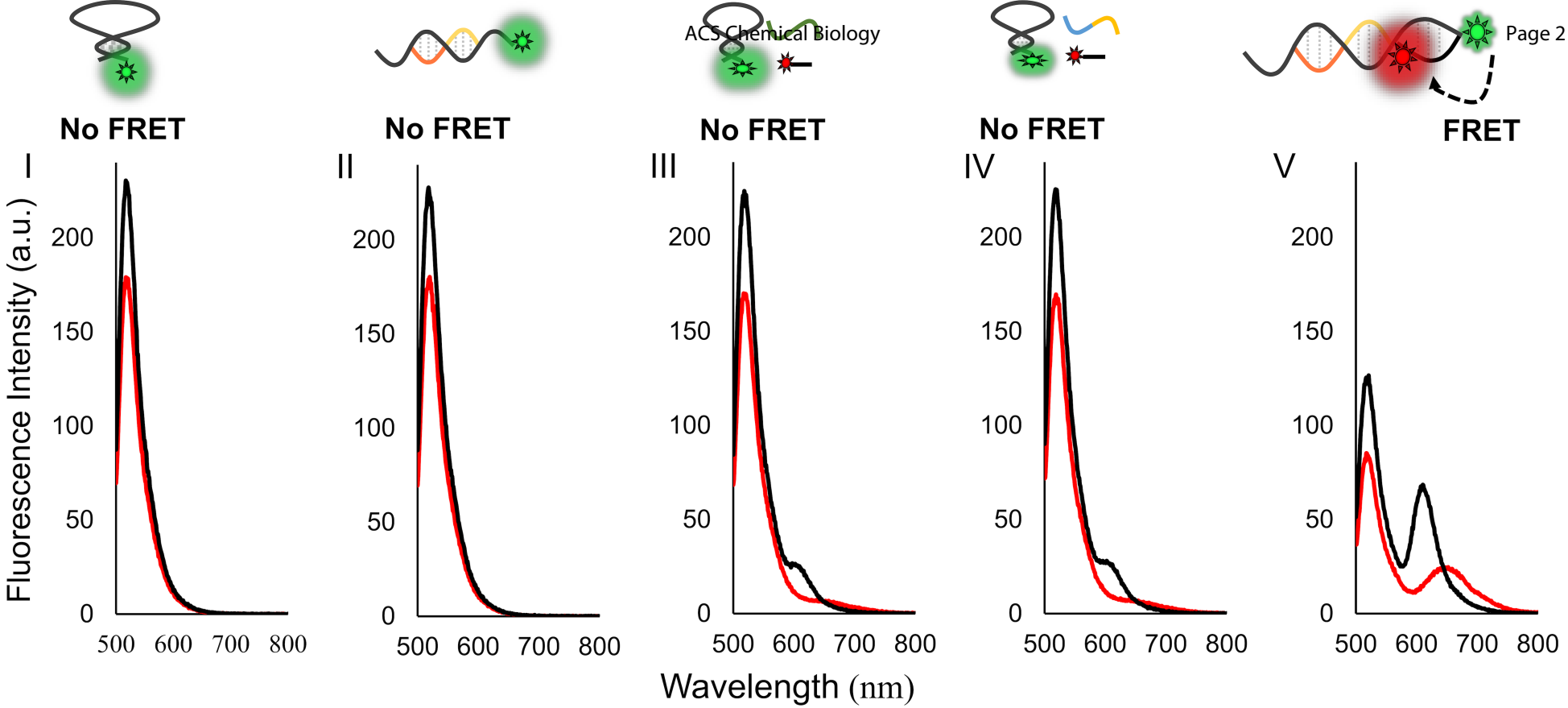

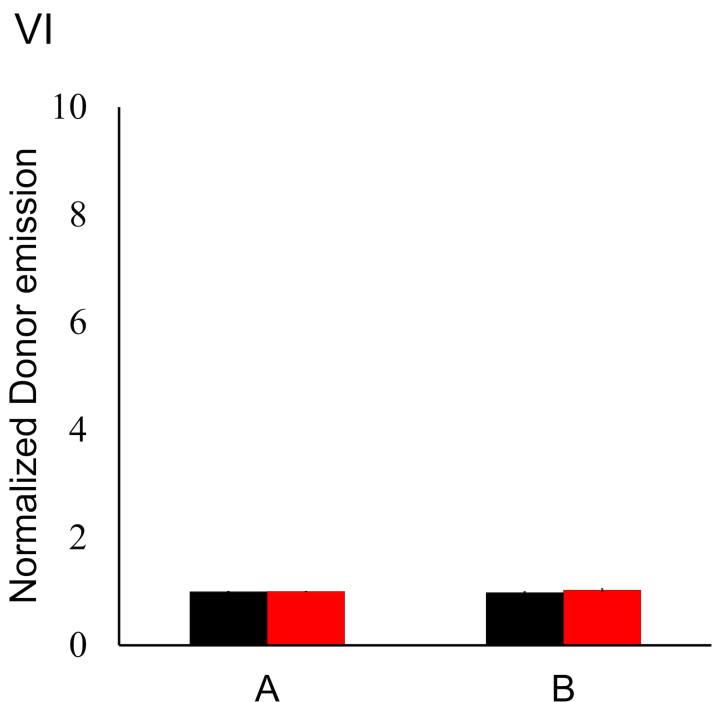

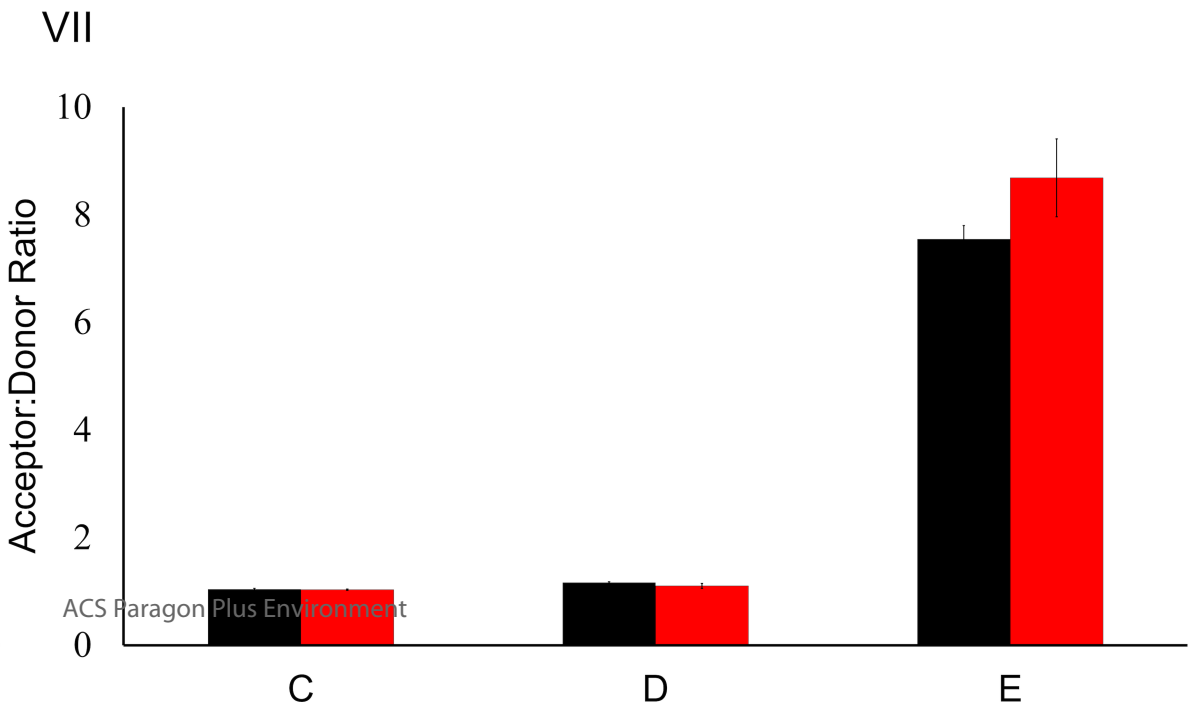

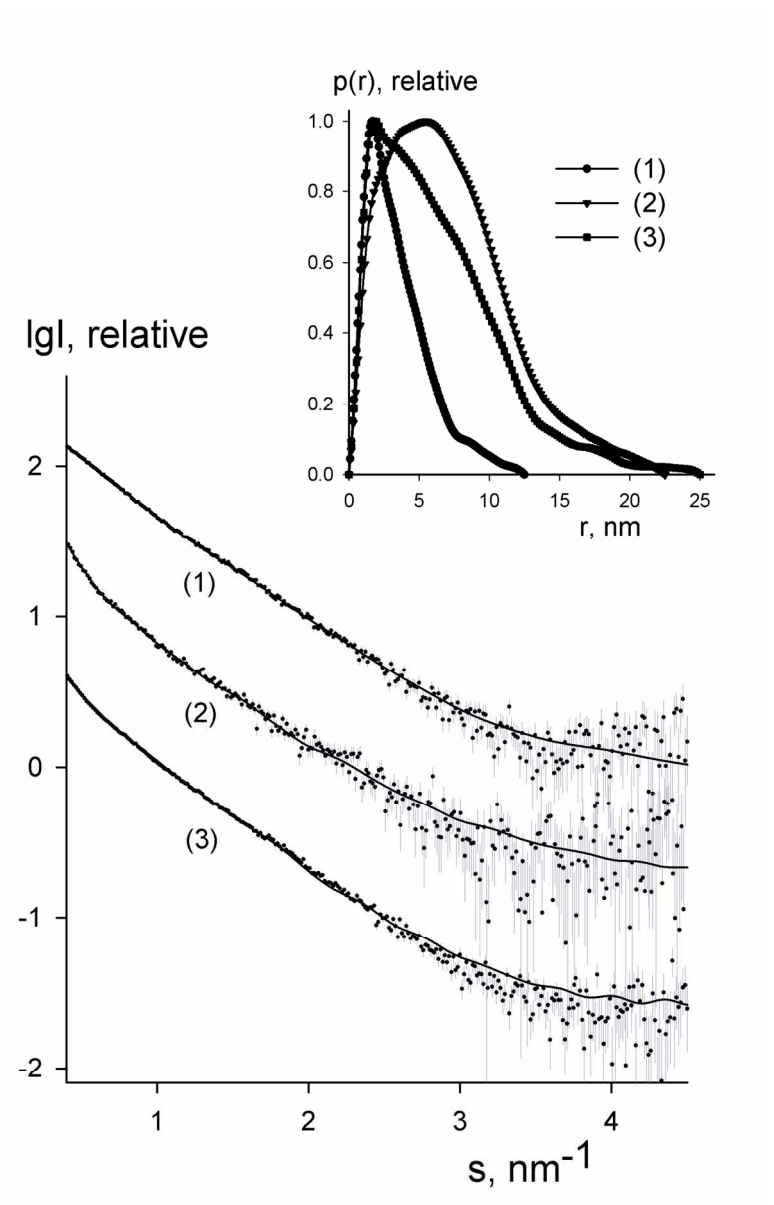

Figure 3

124x193mm (300 x 300 DPI)

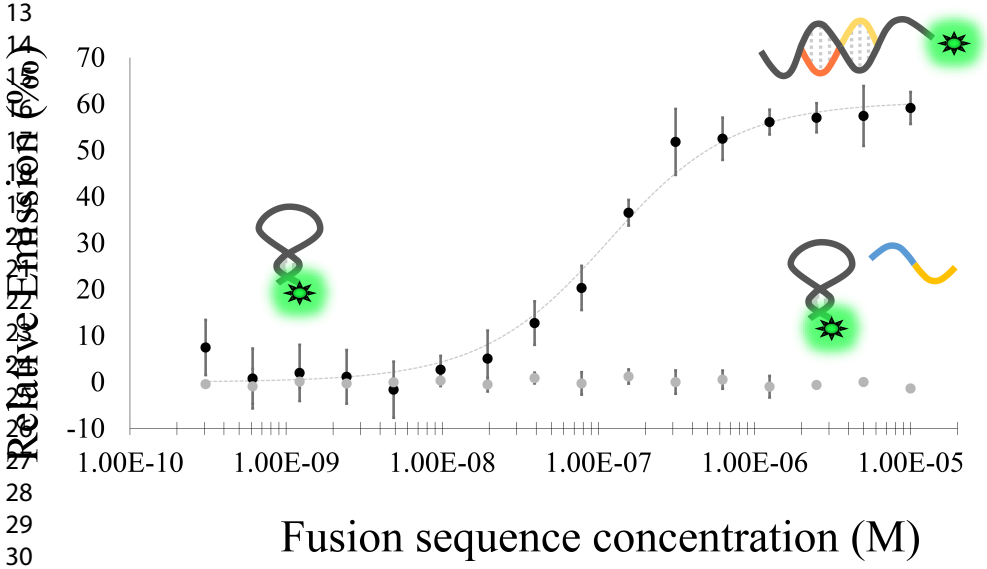
Relative Emission (‰)
70
60
50
40
30
20
10
0
-10
1.00E-10
1.00E-09
1.00E-08
1.00E-07
1.00E-06
1.00E-05
Fusion sequence concentration (M)

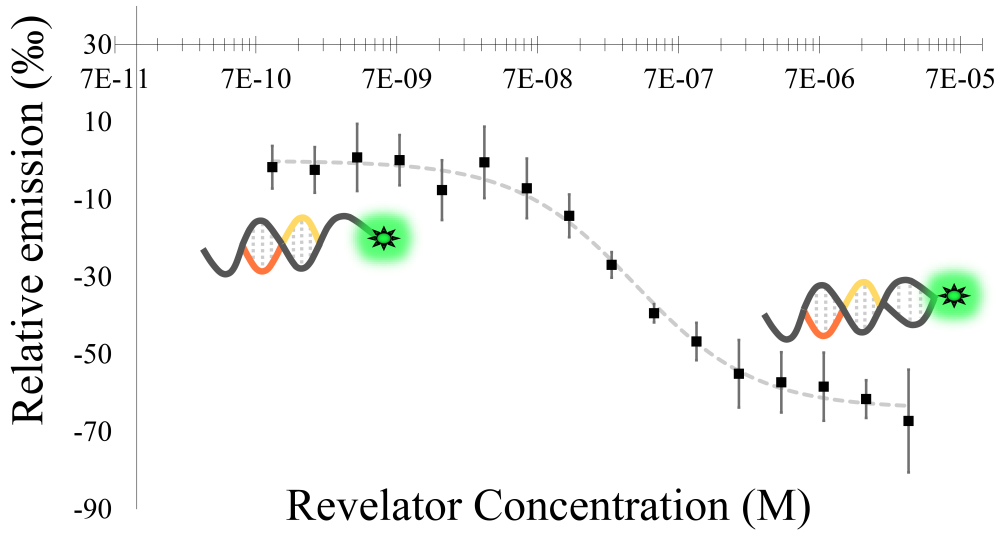
Relative emission (‰)
30
10
-10
-30
-50
-70
-90
7E-11
7E-10
7E-09
7E-08
7E-07
7E-06
7E-05
Revelator Concentration (M)

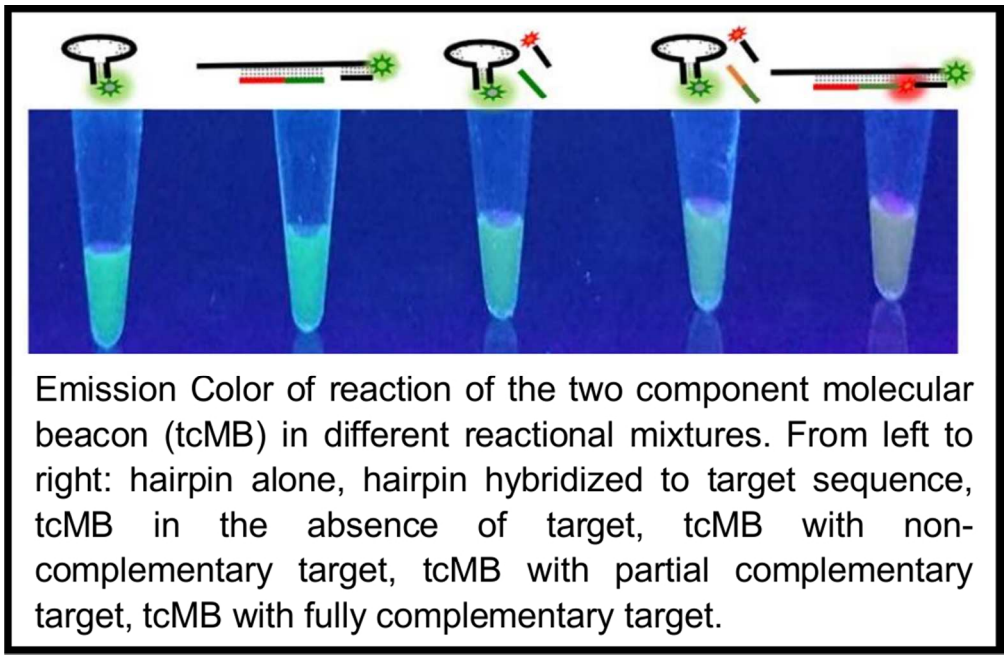

Graphical Abstract - Emission color of the reaction of the two component beacon (tcMB) in different reactions mixtures. From left to right: hairpin alone, hairpin hybridised to a target sequence, tcMB in the absence of a target, tcMB with a non-complementary target, tcMB with a partial target, tcMB with the fully complementary target.

95x62mm (300 x 300 DPI)

Optical and structural characterization of a chronic myeloid leukemia DNA biosensor

Mílton Cordeiro[1,2*], Ana Rita Otrelo-Cardoso[3*], Dmitri I. Svergun[4], Petr V. Konarev[4,5,6], João Carlos Lima[2], Teresa Santos-Silva[3§] and Pedro Viana Baptista[1§]

[1]UCIBIO, Departamento de Ciências da Vida, Faculdade de Ciências e Tecnologia, Universidade Nova de Lisboa, Campus da Caparica, 2829-516 Caparica

[2]LAQV, Departamento de Química, Faculdade de Ciências e Tecnologia, Universidade Nova de Lisboa, Campus da Caparica, 2829-516 Caparica

[3]UCIBIO, Departamento de Química, Faculdade de Ciências e Tecnologia, Universidade Nova de Lisboa, Campus da Caparica, 2829-516 Caparica

[4]European Molecular Biology Laboratory (EMBL), Hamburg Outstation, c/o DESY, Hamburg, Germany, 22067

[5]Shubnikov Institute of Crystallography, Federal Scientific Research Centre "Crystallography and Photonics", Russian Academy of Sciences, Leninsky prospect 59, 119333 Moscow, Russia.

[6]National Research Centre "Kurchatov Institute", pl. Kurchatova 1, 123182 Moscow, Russia.

[*] These authors contributed equally to this work

[§]Corresponding authors: tsss@fct.unl.pt and pmvb@fct.unl.pt

Abstract

Selective base pairing is the foundation of DNA recognition. Here, we elucidate the molecular and structural details of a FRET-based two-component molecular beacon relying on Steady-state Fluorescence Spectroscopy, Small-angle X-ray Scattering (SAXS), Microscale Thermophoresis (MST) and Differential Electrophoretic Mobility. This molecular beacon was designed to detect the most common fusion sequences causing chronic myeloid leukemia, e14a2 and e13a2. The emission spectra indicate that the self-assembly of the different components of the biosensor occurs sequentially, triggered by the fully complementary target. We further assessed the structural alterations leading to the specific fluorescence FRET signature by SAXS, MST and the differential electrophoretic mobility, where the size range observed is consistent with hybridization and formation of a 1:1:1 complex for the probe in the presence of the complementary target and revelator. These results highlight the importance of different techniques to explore conformational DNA changes in solution and its potential to design and characterize molecular biosensors for genetic disease diagnosis.

Introduction

DNA hybridization is a self-assembly process governed by the equilibria of hydrogen bonding, repulsion of the phosphate backbone between the interacting strands, and base stacking interactions [1–4]. These properties are fundamental for the *in vivo* function of DNA and RNA and rule the *in vitro* application of nucleic acids such as biomolecular sensors, gene silencing therapeutics, or 2D/3D nanoscale shapes i.e. as DNA origami [5–7]. DNA sensing technology heavily relies on fluorescence for target detection [8–11]. Amongst the plethora of detection schemes, molecular beacons (MB) provide simultaneously sequence discrimination and signal enhancement via Förster Resonance Energy Transfer (FRET) [12–16]. MB are hybridization-based probes where the FRET distance-dependent phenomenon is applied to detect a specific sequence [17–19]. They are composed of a recognition element made of a single strand DNA molecule (ssDNA), labeled with a fluorophore and a quencher in each extremity. The recognition element is flanked by auto-complementary (palindromic) sequences. Hybridization of the palindromic sequences generates a ssDNA with a hairpin structure where the recognition loop remains single-stranded, available to hybridize to the target sequence. Upon positive recognition, the hairpin structure is disrupted, increasing the distance between the fluorophore and quencher, inducing a partial recovery of emission from the fluorophore [10,19,20]. The spectral signature of FRET is the quenching of donor fluorophore emission, in the case of the dark quencher, or the quenching of the donor with the concomitant increase of the acceptor fluorophore emission. The energy transfer efficiency is highly dependent on the distance between the donor and acceptor (proportional to R^{-6}) and, thus can be used to unravel biological interactions [21,22]. These concepts have been applied in various systems using free oligonucleotides [23,24] and oligonucleotides immobilized in gold nanosurfaces [15,25,26]. These detection probes are highly dependent on their dynamic structure and hybridization efficiency.

The structural characterization of nucleic acid complexes may be achieved in anhydrous samples, using atomic force microscopy or transmission electron microscopy, or in solution using labeled oligonucleotides via fluorescence microscopy/spectroscopy [27]. In the last decade, Small-angle X-ray Scattering (SAXS) has been used to analyze the shape and size of nucleic acids in solution, avoiding the need for extra labeling procedures [28]. There are several examples where SAXS was employed for characterizing the 3D structure of nucleic acid [29,30], to study

DNA interaction with different ions [31]. Recently, Chen et al. [32] used SAXS and FRET to monitor DNA conformations and coordination with histone proteins during the nucleosome core particle disassembly. The combination of these two techniques provides important complementary structural information. FRET is a local structure technique that reports on the relative distance between the two FRET labels while SAXS yields the global structure. When combined, structural changes at local and global scales can be correlated providing an accurate measure of the conformational changes of such system [33]. Although these two techniques have been employed for the characterization of a protein-based biosensor [34], to the best of our knowledge, no similar approach had been used for DNA based biosensors whose output relies on the interaction of several DNA elements. Such approach is of relevance to support the mechanistic interpretation of the events taking place upon recognition. Here, we take advantage of these two perspectives to characterize the designed two-component MB, whose assembly is triggered by the presence of sequences derived from the aberrant gene fusion responsible for chronic myeloma leukemia (CML). The molecular hallmark of CML is the Philadelphia chromosome, that results from a reciprocal translocation between chromosome 9 and 22 [35]. This translocation generates the fusion gene BCR-ABL which, by alternative splicing, originates the variants e14a2 and e13a2, observed in 95% of the positive CML diagnosed cases. The local and global analyses were complemented with differential electrophoretic mobility and microscale thermophoresis.

Results and discussion

Conceptual definition of the biosensor. The developed two-component FRET-based biosensors were designed to selectively discriminate between the variants e14a2 and e13a2 observed in CML. The loop portion (recognition element) of the donor labeled hairpin probes are complementary to specific fusion sequence of e14a2 and e13a2 (e14A and e13A, respectively) (Figure 1 and Table 1). The hybridization of the hairpin (e14A/e13A) with the target sequence (e14B/e13B), disrupts this secondary structure, exposing the palindromic sequence (Figure 1B). Then, an acceptor-labeled revelator (e14C/e13C) can hybridize to this region – Figure 1C. The

hybridization of the revelator sequence approximates the donor and acceptor pair to distances compatible with energy transfer.

The free energy of the hairpin formation, hybridization to the target sequence and the three-component complex was estimated using the software package NUPACK [36,37] – see Table S1 for the simulated hybridization events.

Insert Figure 1.

Insert Table 1.

Design of the biosensor and fluorophore selection. The fluorophores used for labeling were selected based on their absorption and emission wavelengths to ensure efficient FRET pairing. Experimental data show that, upon hybridization of the revelator, the relative orientations of donor and acceptor transition dipole moments do not hinder energy transfer [38]. Two different acceptors, with distinct emission spectra (Dy and ROX), were used to label the revelator sequences and differentiate between the target sequences – e14B and e13B, respectively. The absorption spectra of both acceptors display a significant overlap with the emission spectra of the donor (6-FAM), ensuring that, upon formation of each ABC complex, a FRET signature is observed (Figure S1 the absorption/emission spectra of each fluorophore). Using the software PhotoChemCad [39], the critical Förster radius (R0) of each pair was predicted: 55.86 Å for FAM/ROX and 59.41 Å for FAM/Dy). These R0 values are compatible with the occurrence of FRET in the final ensemble considering a theoretical separation between donor and acceptor of 34 Å in the final complex (assuming a base separation of 3.4 Å [40] and a stem portion of 10 bp).

The sample excitation was performed at 495 nm, which corresponds to the maximum donor absorption. The absorption spectra of the acceptors also reveal residual absorption at this wavelength, which leads to the cross-excitation of the acceptors. This phenomenon is not desirable but inevitable since the overlap between the emission spectrum of the donor and the absorption spectra of the acceptors is a requirement for energy transfer. Moreover, the selected fluorophores have relatively wide emission/absorption spectra and the donor presents a small

Stokes shift. Nonetheless, these fluorophore pairs can generate distinguishable FRET signals from the direct excitation of the donor.

Analysis of the complex assembly. The sequential assembly of the designed sensor is required to detect the fusion sequence. The formation of the labeled DNA complexes was evaluated by FRET, while the conformational changes of the individual components and the final ensemble, determined by SAXS. The samples measured by SAXS are fluorophore-free since the presence of the label is not required for this technique and does not affect the overall structure of the oligonucleotides in solution.

The basal fluorescence of the donor e14A and e13A was determined in the absence of the target (e14B and e13B) and acceptor (e14C and e13C) – Figure 2.I. The scattering profile for the two labeled-free hairpin molecules results in R_g and D_{max} values that are concordant with a 43 nt sequence, assuming a symetrical hairpin conformation with a base separation of 3.4 Å [41]. The obtained parameters are slightly higher for hairpin e14A (R_g 2.93 nm and D_{max} 12.5 nm) than e13A (R_g of 2.36 nm and D_{max} of 8.0 nm) suggesting that the latter is more compact (Table 2 and Figure 3). This corroborates the NUPACK *in silico* predictions where e13A has a higher self-complementarity level than e14A, inferred by the lower free Gibbs energy – see Table S1.

Insert Figure 2.

Insert Figure 3.

The effect of the target sequence hybridization to the donor labeled hairpin emission was assessed for both variants (Figure 2.II.). The obtained spectra show that the presence of the complementary target has no measurable impact on the emission spectrum of the donor. However, the scattering curves show a significant structural alteration, with an increase of the R_g and D_{max} parameters (R_g of 5.85 nm and D_{max} of 22.5 nm for e14AB; and R_g of 5.40 nm and D_{max} of 20.0 nm for e13AB) – Table 2. This variation is due to the disruption of the symmetrical hairpins upon hybridization to the target molecule, forming a more extended structure (Figure 3 and Figure S2).

Insert Table 2.

The formation of the AB complexes is supported by the different electrophoretic mobility profile depicted in Figure S3. Here, the e14AB (RF= 0.181) and the e13AB (RF= 0.177) complex have a lower migration when compared to the hairpin alone (with RF of 1 for e14A and e13A). MST results are also in agreement, showing that a strong binding is observed upon formation of the hairpin-target formation (K_D of 10.0 (± 2.0) × 10^{-8} M) – Figure 4.

Insert Figure 4.

Emission spectra were also collected for the donor labeled hairpin in the presence of both revelators and a non-related target (no complementarity with any of the hairpins, as this sequence shows an identity of 18.2 % and 28.6% towards the e13B and e14B, respectively) – Figure 2.III. This scenario corresponds to the negative control that provides the background emission of the acceptors (due to direct excitation), to be used as a baseline for evaluating the acceptor emission enhancement in the presence of FRET. In this case, the donor emission of e14AYC overlaps with the donor emission of e14A and e14AB, indicating the absence of FRET (Figure 2.VI). Considering the non-complementarity between the loop region of the hairpin and the non-related target, no structural variation is expected in this scenario and SAXS data were not collected.

To test the specificity of the designed system, the target sequences, which share 55.6% of sequence identity, were incubated with the non-corresponding hairpins: e14A-e13B-e14C and e13A-e14B-e13C. The spectral signature obtained in each case is the same as the negative control, indicating that the hybridization between the three strands did not occur (Figure 2.IV.). The absence of interaction is corroborated by mobility analysis in acrylamide gel electrophoresis (Figure S3) and by the MST profile, where a concentration-dependent thermophoresis is not observed (Figure 4). However, the structural parameters obtained for these cases, R_g and D_{max}

values (e14A-e13B-e14C: R_g of 3.80 nm and D_{max} of 14.00 nm; e13A-e14B-e13C: R_g of 3.95 nm and D_{max} of 18.00 nm), are higher than the ones obtained for the hairpins alone (e14A: R_g of 2.93 nm and D_{max} of 8.0 nm; e13A R_g of 2.36 nm and D_{max} of 12.5 nm), which might result from the presence of free molecules in solution (Table 2). It should be noted that the concentrations and temperature conditions needed to perform each type of measurements are very different. For the scattering experiments, data is collected at low temperature and at concentrations ~×100 higher than that of fluorescence spectroscopy and MST, which could induce the hybridization of the hairpin with the partial complementary target [42], as simulated by the NUPACK software – Table S1.

To form the final complex, the three components of the sensor are combined, producing a stable ABC ensemble. In this case, the presence of a fully complementary target and revelator results in a specific FRET signal distinguishable from the other scenarios. The fully complementary target (Figure 2.V.), promotes a sharp decrease of the donor emission and the concomitant increase of the acceptor emission. Considering that an equimolar concentration of donor/acceptors was kept constant in all conditions, this clear FRET signature indicates the hybridization of the three strands. Considering the e14ABC complex, the donor channel displays a 48% emission in comparison to the donor in the absence of FRET (Figure 2.V.), which corresponds to 52% energy transfer for the 6-FAM/Dy pair. The MST assay shows the formation of a tight complex (with K_D of 3.3× 10^{-7} (± 4.4× 10^{-8}) M) and the melting profile (Figure S4), at high temperature, shows a steep signal variation only in the presence of a fully complementary target. This profile is due to the disassembly of the ensemble (ABC complex). The signal variation in the control reactions shows the intrinsic temperature variation of the fluorophores, with the signals (donor and acceptor) of all the scenarios converging at high temperature.

Similar results were obtained for e13, where the donor emission in the e13ABC complex presents 55% emission of the e13A alone (Figure S2.V.). This corresponds to 45% of energy transfer for the 6-FAM/ROX pair. In both cases, the assessment of the acceptor enhancement was determined after subtracting the donor emission band. The energy transfer efficiency

determined experimentally is highly dependent on the hybridization efficiency of the target molecule to the hairpin, as well as the revelator hybridization to the hairpin+target complex. This might explain the deviation from the theoretical efficiency of 95.34% for the pair 6-FAM/ROX and 96.6% for the pair 6-FAM/DY-520XL MegaStokes (calculated using PhotoChemCAD [39], considering a refractive index of 1.333, an orientation factor k^2=0.6666 and a fluorescence quantum yield of 0.79 for FAM [43]. For the acceptors, the experimentally assessed extinction coefficients were 70712 M^{-1} cm^{-1} at 583 nm for ROX (Figure S5 A) and 44924 M^{-1} cm^{-1} at 542 nm for Dy-520 XI Mega Stokes (Figure S5B). A 4-fold increase was observed for both acceptors which correspond to a ~7.5 fold increase in the ratio of the acceptor and donor channels – ratiometric analysis (Figure 2.VII).

SAXS results support the fluorescence spectroscopic observations, where the R_g and D_{max} values obtained for e14ABC and e13ABC (R_g: 5.21 and 4.56 nm, D_{max}: 20 and 18 nm, respectively) are higher than the ones obtained for the corresponding isolated hairpins (e14A and e13A), as expected for an open hairpin hybridized with its target sequence (Table 2). Furthermore, these values are slightly lower than the ones observed for e14A-e14B or e13A-e13B, due to the formation of a more compact structure upon the duplex formation at the 3' end of the open hairpin (Figure S2). This is also observed in the electrophoretic profile, where the complexes (e14ABC and e13ABC - (lane 3 of Figure S3.A and B, respectively)) migrate beyond the e14AB or e13AB pairs (lane 2 of Figure S3.A and B, respectively).

The combined use of the different biophysical techniques in this study provides important complementary structural information about the designed sensor. The hybridization of the three strands occurs sequentially, with the hybridization of the acceptor-labeled oligonucleotide depending on the pre-hybridization of the target; each hybridization step induces an alteration of the thermophoresis profile. The system can discriminate between the two variants, even in the presence of a partially complementary target with 52.4% identity, resulting in the lack of a FRET signal, the absence of a concentration-dependent thermophoresis signal, and a similar electrophoretic profile as the hairpin alone. These results demonstrate that FRET combined with

SAXS allows the evaluation of structural changes at local and global scales and provide an accurate measure of the conformational change of the molecular sensor.

Conclusions

Here, we show the potential use of FRET, MST, Differential Electrophoretic Mobility and SAXS to reveal the dynamics of DNA hybridization in a two-component FRET-based molecular beacon. This study indicates that the formation of a final donor-target-revelator complex is sequential and sequence-specific. The alteration of the thermophoretic mobility upon target and revelator binding supports the formation of the complex. SAXS indicates that upon target recognition, the size of the intermediary is larger than the hairpin. Data also suggest the formation of a stable ternary complex, with a slight size decrease after the hybridization of the revelator, as supported by electrophoretic and thermophoretic mobility profiles. This work describes a methodology that can be used to design and characterize molecular actuators and sensors, such as beacons for fast and accurate detection of genetic alterations.

Experimental Methods

All reagents were of analytical grade and purchased from Sigma-Aldrich (Germany). All buffers were filtered through an Acrodisc® Syringe Filter 0.2 µm Supor® membrane Pall, United States of America). The oligonucleotides were purchased from STABVIDA (Portugal) and used without further purification.

Hairpin design and target sequences. Each ssDNA was designed to generate a hairpin structure. The loop portions are composed by the complementary sequences of the BCR-ABL fusion regions – e14a2 and e13a2 transcript sequences (accession numbers AJ131466.1 and AJ131467.1, respectively), herein designated as e14A and e13A. The sequences were optimized using the hybridization predictor software NUPACK [36]. To evaluate the reactivity towards different target sequences and infer the structural alterations upon complex formation, oligonucleotide targets were designed to obtain different degrees of complementarity. The e14a2 and e13a2 fusion sequences were used as complementarity targets (herein designated as e14B and e13B, respectively), while a non-related sequence (designated as Y) was used to obtain non-complementary target (negative control). The revelators were designed to hybridize to the palindrome sequence of each hairpin (herein designated as e14C and e13C).

Fluorophore selection. Donor and the acceptors were chosen based on their spectral properties. 6-carboxyfluorescein (6-FAM) was selected as donor fluorophore to label e14A and e13A hairpins. DY-520XL MegaStokes (Dy) and 5-carboxy-X-rhodamine (ROX) and were chosen as acceptors and used to label the e14C and e13C revelators, respectively.

Complex formation and fluorescence evaluation. Hybridization of the hairpins to their respective target sequences was carried out in 0.5× TBE pH 8.3 and 154 mM NaCl, using 0.75 μM of each component. The reactants were incubated for 30 s at 368 K, followed by 20 min at 293 K. Emission spectra were collected from 500 to 800 nm upon sample excitation at 495 nm. A temperature-dependent profile was also gathered for each condition after the described incubation periods (Figure S4).

Fluorescence analysis. Fluorescence emission spectra were collected on a Varian Cary Eclipse Fluorescence Spectrophotometer (Agilent Technologies, United States of America) with 5 nm bandwidth excitation and emission slits using a 3-mm optical path quartz cuvette (HELLMA, Germany). Sample excitation was performed at 495 nm, and fluorescence measurements were performed at 293K. A positive FRET signal consists in the decrease of the donor band with the increase of the fluorescence band of the acceptors, using the negative control as fluorescence baseline. The energy efficiency was determined by the degree of quenching of the donor emission in comparison to the donor blank. The donor channel was defined as the spectral range between 501 and 580 nm, the acceptor 1 (DY-520XL MegaStokes – Dy) channel from 600 to 800 nm and acceptor 2 (5-carboxy-X-rhodamine – 5-ROX) channel from 581 to 680 nm. The integrated donor signal was normalized to the fluorescence signal of the donor in the donor blank reaction. The integrated acceptor signal was normalized to the fluorescence signal of the acceptor in the negative reaction. The ratiometric analysis was performed through the ratio between the acceptor and donor channel.

Microscale Thermophoresis (MST). The binding affinity of the hairpin-target hybridization was determined in 0.5 × TBE pH 8.0 and 154 mM NaCl. 30 nM of the 6-FAM labeled hairpin was titrated with increasing concentrations of the complementary target (from 10 μM to 0.03 nM).

For the binding affinity of the revelator, 30 nM of the 6-FAM labeled hairpin was pre-hybridized to the complementary target sequence and titrated with the unlabeled revelator using an upper limit of 30 μM and a lower limit of 0.92 nM. The measurements were performed in a NanoTemper Monolith NT.115 at 293 K using the blue LED power at 60% and the infrared laser (1480 nm). The solution was irradiated with IR laser for 20 seconds. The samples were measured in high purity glass capillaries (NT.115 Standard Treated Capillaries from NanoTemper Technologies).

SAXS data collection and analysis. The SAXS experiments were performed at EMBL P12 beamline, DESY, Hamburg, Germany [44] and at EMBL BM29 beamline, ESRF, Grenoble, France [45]. Each individual non-labeled component (e13A, e14A, e13B, e14B, e13C and e14C) and each hybridization event (e13AB, e14AB, e14A-e13B-e14C, e13A-e14B-e13C, e13ABC and e14ABC) were measured at 283 K, except e13A, e13B and e13C that were measured at 277 K, using serial dilutions from 2 mg/mL to 0.25 mg/mL. The data collected at P12 beamline was recorded using a Pilatus 2M detector (DECTRIS, Switzerland) with 20 x 0.05 s exposure time, at sample-detector distance 3.00 m and wavelength 1.24 Å. The data at BM29 beamline were recorded using a Pilatus 1M detector with 10 x 1 s exposure time, with a sample-detector distance 2.87 m and wavelength 0.99 Å. No measurable radiation damage was detected by comparison of successive time frames. The primary data reduction was performed automatically by the pipeline software [46]. The data were processed with the ATSAS package [47] using standard procedures, corrected for buffer contribution, and extrapolated to infinite dilution using PRIMUS [48] software. GNOM [49] was used to provide the $P(r)$ and determine the corresponding maximum particle size (D_{max}) and the radius of gyration (R_g). The excluded volume of the hydrated DNA molecule (V_P) was calculated using the Porod approximation [50].

Supporting Information

This material is available free of charge via the internet at http://pubs.acs.org.

Table S1. In silico simulations of the designed sequences;

Figure S1. Normalized absorption/emission spectra of the used fluorophores;

Figure S2. Experimental SAXS patterns and scattering calculated from the ab initio models;

Figure S3. Acrylamide gel electrophoresis of the tested scenarios;

Figure S4. Melting profile of the tested condition;

Figure S5. Acceptors extinction coefficient determination.

Accession codes

The collected SAXS data and the generated models have been deposited and are available at Small-Angle Scattering Biological Data Bank (SASBDB), under the codes: SASDC95 - e14A; SASDCA5 - e14B; SASDCB5 - e14C; SASDCC5 - e14AB; SASDCD5 - e14ABC; SASDCE5 - e13A; SASDCF5 - e13B; SASDCG5 - e13C; SASDCH5 - e13AB; SASDCJ5 - e13ABC; SASDCK5 - e13Ae14Be13C; SASDCL5 - e14Ae13Be14C.

Acknowledgments

This work was supported by the Unidade de Ciências Biomoleculares Aplicadas-UCIBIO which is financed by national funds from FCT/MEC (UID/Multi/04378/2013) and co-financed by the ERDF under the PT2020 Partnership Agreement (POCI-01-0145-FEDER-007728), and PTDC/QEQ-MED/1902/2014. ARO-C and MC thank FCT/MEC for SFRH/BD/85806/2012 and SFRH/BD/87836/2012, respectively.

The authors thank the EMBL P12 (DESY, Hamburg, Germany) and BM29 (ESRF, Grenoble, France) beamline staff for assistance during data collection.

References

(1) Suckling, C. J. Molecular Recognition - A Universal Molecular Science? *Experientia* **1991**, *47*, 1093–1095.

(2) Pinheiro, A. V; Han, D.; Shih, W. M.; Yan, H. Challenges and Opportunities for Structural DNA Nanotechnology. *Nat. Nanotechnol.* **2011**, *6*, 763–772.

(3) Alhambra, C.; Luque, F. J.; Gago, F.; Orozco, M. Ab Initio Study of Stacking Interactions in A- and B-DNA. *J. Phys. Chem. B* **1997**, *5647*, 3846–3853.

(4) Bansal, M. DNA Structure : Revisiting the Watson – Crick Double Helix. *Curr. Sci.* **2003**, *85*, 1556–1563.

(5) Cordeiro, M.; Ferreira Carlos, F.; Pedrosa, P.; Lopez, A.; Baptista, P. Gold Nanoparticles for Diagnostics: Advances towards Points of Care. *Diagnostics* **2016**, *6*, 43.

(6) Song, J.; Zhang, Z.; Zhang, S.; Liu, L.; Li, Q.; Xie, E.; Gothelf, K. V.; Besenbacher, F.; Dong, M. Isothermal Hybridization Kinetics of DNA Assembly of Two-Dimensional DNA Origami. *Small* **2013**, *9*, 2954–2959.

(7) Tørring, T.; Voigt, N. V.; Nangreave, J.; Yan, H.; Gothelf, K. V. DNA Origami: A Quantum Leap for Self-Assembly of Complex Structures. *Chem. Soc. Rev.* **2011**, *40*, 5636–5646.

(8) Wang, K.; Tang, Z.; Yang, C. J.; Kim, Y.; Fang, X.; Li, W.; Wu, Y.; Medley, C. D.; Cao, Z.; Li, J.; Colon, P.; Lin, H.; Tan, W. Molecular Engineering of DNA: Molecular Beacons. *Angew. Chemie - Int. Ed.* **2009**, *48*, 856–870.

(9) Pickup, J. C.; Hussain, F.; Evans, N. D.; Rolinski, O. J.; Birch, D. J. S. Fluorescence-Based Glucose Sensors. *Biosens. Bioelectron.* **2005**, *20*, 2555–2565.

(10) Zheng, J.; Yang, R.; Shi, M.; Wu, C.; Fang, X.; Li, Y.; Li, J.; Tan, W. Rationally Designed Molecular Beacons for Bioanalytical and Biomedical Applications. *Chem. Soc. Rev.* **2015**, *44*, 3036–3055.

(11) Sieroń, A.; Sieroń-Stołtny, K.; Kawczyk-Krupka, A.; Latos, W.; Kwiatek, S.; Straszak, D.; Bugaj, A. M. The Role of Fluorescence Diagnosis in Clinical Practice. *Onco. Targets. Ther.* **2013**, *6*, 977–982.

(12) Yang, L.-H.; Ahn, D. J.; Koo, E. Ultrasensitive FRET-Based DNA Sensor Using PNA/DNA Hybridization. *Mater. Sci. Eng. C* **2016**, *69*, 625–630.

(13) Zhang, C.; Hu, J. Single Quantum Dot-Based Nanosensor for Multiple DNA Detection.

Anal. Chem. **2010**, *82*, 1921–1927.

(14) Cordeiro, M.; Giestas, L.; Lima, J. C.; Baptista, P. Coupling an Universal Primer to SBE Combined Spectral Codification Strategy for Single Nucleotide Polymorphism Analysis. *J. Biotechnol.* **2013**, *168*, 90–94.

(15) Cordeiro, M.; Giestas, L.; Lima, J.; Baptista, P. BioCode Gold-Nanobeacon for the Detection of Fusion Transcripts Causing Chronic Myeloid Leukemia. *J. Nanobiotechnology* **2016**, *14*, 38.

(16) Koch, W. H. Technology Platforms for Pharmacogenomic Diagnostic Assays. *Nat. Rev. Drug Discov.* **2004**, *3*, 749–761.

(17) Tyagi, S.; Kramer, R. Molecular Beacons: Probles That Fluoresce upon Hybridization. *Nat. Biotechnol.* **1996**, *14*, 303–306.

(18) Marras, S. A. E.; Tyagi, S.; Kramer, F. R. Real-Time Assays with Molecular Beacons and Other Fluorescent Nucleic Acid Hybridization Probes. *Clin. Chim. Acta* **2006**, *363*, 48–60.

(19) Navarro, E.; Serrano-Heras, G.; Castaño, M. J.; Solera, J. Real-Time PCR Detection Chemistry. *Clin. Chim. Acta* **2015**, *439*, 231–250.

(20) Singh, J.; Kaur, H.; Kaushik, A.; Peer, S. A Review of Antisense Therapeutic Interventions for Molecular Biological Targets in Various Diseases. *Int J Pharmacol* **2011**, 294–315.

(21) Lakowicz, J. R. *Principles of Fluorescence Spectroscopy*, 3 nd.; Academic, K., Ed.; Plenum Publishers: New York, 2006.

(22) Beljonne, D.; Curutchet, C.; Scholes, G. D.; Silbey, R. J. Beyond Förster Resonance Energy Transfer in Biological and Nanoscale Systems. *J. Phys. Chem. B* **2009**, *113*, 6583–6598.

(23) Thelwell, N.; Millington, S.; Solinas, A.; Booth, J.; Brown, T. Mode of Action and Application of Scorpion Primers to Mutation Detection. *Nucleic Acids Res.* **2000**, *28*, 3752–3761.

(24) Nazarenko, I. A.; Bhatnagar, S. K.; Hohman, R. J. A Closed Tube Format for Amplification and Detection of DNA Based on Energy Transfer. *Nucleic Acids Res.* **1997**, *25*, 2516–2521.

(25) Rosa, J.; Conde, J.; de la Fuente, J. M.; Lima, J. C.; Baptista, P. V. Gold-Nanobeacons for Real-Time Monitoring of RNA Synthesis. *Biosens bioelectron* **2012**, *36*, 161–167.

(26) Song, S.; Liang, Z.; Zhang, J.; Wang, L.; Li, G.; Fan, C. Gold-Nanoparticle-Based Multicolor Nanobeacons for Sequence-Specific DNA Analysis. *Angew. Chemie* **2009**, *48*, 8670–8674.

(27) Scheible, M.; Jungmann, R.; Simmel, F. C. Assembly and Microscopic Characterization of DNA Origami Structures. In *Adv Exp Med Biol.*; Springer: Netherlands, 2012; Vol. 733, pp 87–96.

(28) Lipfert, J.; Doniach, S. Small-Angle X-Ray Scattering from RNA, Proteins, and Protein Complexes. *Annu. Rev. Biophys. Biomol. Struct.* **2007**, *36*, 307–327.

(29) Meisburger, S. P.; Pabit, S. A.; Pollack, L. Determining the Locations of Ions and Water around DNA from X-Ray Scattering Measurements. *Biophys. J.* **2015**, *108*, 2886–2895.

(30) Fischer, S.; Hartl, C.; Frank, K.; Rädler, J. O.; Liedl, T.; Nickel, B. Shape and Interhelical Spacing of DNA Origami Nanostructures Studied by Small-Angle X-Ray Scattering. *Nano Lett.* **2016**, *16*, 4282–4287.

(31) Pollack, L. SAXS Studies of Ion–Nucleic Acid Interactions. *Annu. Rev. Biophys.* **2011**, *40*, 225–242.

(32) Chen, Y.; Tokuda, J. M.; Topping, T.; Meisburger, S. P.; Pabit, S. A.; Gloss, L. M.; Pollack, L. Asymmetric Unwrapping of Nucleosomal DNA Propagates Asymmetric Opening and Dissociation of the Histone Core. *PNAS* **2017**, *114*, 334–339.

(33) Andresen, K.; Jimenez-Useche, I.; Howell, S. C.; Yuan, C.; Qiu, X. Solution Scattering and FRET Studies on Nucleosomes Reveal DNA Unwrapping Effects of H3 and H4 Tail Removal. *PLoS One* **2013**, *8,* e78587.

(34) Mertens, H.; Piljić, A.; Schultz, C.; Svergun, D. Conformational Analysis of a Genetically Encoded FRET Biosensor by SAXS. *Biophys. J.* **2012**, *102*, 2866–2875.

(35) Hanfstein, B.; Lauseker, M.; Hehlmann, R.; Saussele, S.; Erben, P.; Dietz, C.; Fabarius, A.; Proetel, U.; Schnittger, S.; Haferlach, C.; Krause, S.W.; Schubert, J.; Einsele, H.; Hänel, M.; Dengler, J.; Falge, C.; Kanz, L.; Neubauer, A.; Kneba, M.; Stegelmann, F.; Pfreundschuh, M.; Waller, C. F.; Spiekermann, K.; Baerlocher, G. M.; Pfirrmann, M.; Hasford, J.; Hofmann, W. K.; Hochhaus, A.; Müller, M. C.; SAKK and the German CML

Study Group. Distinct Characteristics of e13a2 versus e14a2 BCR-ABL1 Driven Chronic Myeloid Leukemia under First-Line Therapy with Imatinib. *Haematologica* **2014**, *99*, 1441–1447.

(36) Zadeh, J. N.; Steenberg, C. D.; Bois, J. S.; Wolfe, B. R.; Pierce, M. B.; Khan, A. R.; Dirks, R. M.; Pierce, N. A. NUPACK: Analysis and Design of Nucleic Acid Systems. *J. Comput. Chem.* **2011**, *32*, 170–173.

(37) Dirks, R. M.; Bois, J. S.; Schaeffer, J. M.; Winfree, E.; Pierce, N. A. Thermodynamic Analysis of Interacting Nucleic Acid Strands. *SIAM Rev.* **2007**, *49* 65–88.

(38) Sindbert, S.; Kalinin, S.; Nguyen, H.; Kienzler, A.; Clima, L.; Bannwarth, W.; Appel, B.; Müller, S.; Seidel, C. A. M. Accurate Distance Determination of Nucleic Acids via Förster Resonance Energy Transfer: Implications of Dye Linker Length and Rigidity. *J. Am. Chem. Soc.* **2011**, *133*, 2463–2480.

(39) Du, H.; Fuh, R.-C. A.; Li, J.; Corkan, L. A.; Lindsey, J. S. PhotochemCAD: A Computer-Aided Design and Research Tool in Photochemistry. *Photochem. Photobiol.* **1998**, *68*, 141–142.

(40) Tinland, B.; Pluen, A.; Sturm, J.; Weill, G. Persistence Length of Single-Stranded DNA. *Macromolecules* **1997**, *30*, 5763–5765.

(41) Chi, Q.; Wang, G.; Jiang, J. The Persistence Length and Length per Base of Single-Stranded DNA Obtained from Fluorescence Correlation Spectroscopy Measurements Using Mean Field Theory. *Phys. A Stat. Mech. its Appl.* **2013**, *392*, 1072–1079.

(42) Markegard, C. B.; Gallivan, C. P.; Cheng, D. D.; Nguyen, H. D. Effects of Concentration and Temperature on DNA Hybridization by Two Closely Related Sequences via Large-Scale Coarse-Grained Simulations. *J. Phys. Chem. B* **2016**, *120*, 7795–7806.

(43) Rosa, J.; Lima, J. C.; Baptista, P. V. Experimental Photophysical Characterization of Fluorophores in the Vicinity of Gold Nanoparticles. *Nanotechnology* **2011**, *22*, 415202.

(44) Blanchet, C. E.; Spilotros, A.; Schwemmer, F.; Graewert, M. A.; Kikhney, A.; Jeffries, C. M.; Franke, D.; Mark, D.; Zengerle, R.; Cipriani, F.; Fiedler, S.; Roessle, M.; Svergun, D. I. Versatile Sample Environments and Automation for Biological Solution X-Ray Scattering Experiments at the P12 Beamline (PETRA III, DESY). *J. Appl. Crystallogr.* **2015**, *48*, 431–443.

(45) Pernot, P.; Round, A.; Barrett, R.; De Maria Antolinos, A.; Gobbo, A.; Gordon, E.; Huet, J.; Kieffer, J.; Lentini, M.; Mattenet, M.; Morawe, C.; Mueller-Dieckmann, C.; Ohlsson, S.; Schmid, W.; Surr, J.; Theveneau, P.; Zerrad, L.; McSweeney, S. Upgraded ESRF BM29 Beamline for SAXS on Macromolecules in Solution. *J. Synchrotron Radiat.* **2013**, *20*, 660–664.

(46) Franke, D.; Kikhney, A. G.; Svergun, D. I. Automated Acquisition and Analysis of Small Angle X-Ray Scattering Data. *Nucl. Instruments Methods Phys. Res. Sect. A Accel. Spectrometers, Detect. Assoc. Equip.* **2012**, *689*, 52–59.

(47) Petoukhov, M. V; Franke, D.; Shkumatov, A. V; Tria, G.; Kikhney, A. G.; Gajda, M.; Gorba, C.; Mertens, H. D. T.; Konarev, P. V; Svergun, D. I. New Developments in the ATSAS Program Package for Small-Angle Scattering Data Analysis. *J. Appl. Crystallogr.* **2012**, *45*, 342–350.

(48) Konarev, P. V.; Volkov, V. V.; Sokolova, A. V.; Koch, M. H. J.; Svergun, D. I. *PRIMUS* : A Windows PC-Based System for Small-Angle Scattering Data Analysis. *J. Appl. Crystallogr.* **2003**, *36*, 1277–1282.

(49) Svergun, D. I. Determination of the Regularization Parameter in Indirect-Transform Methods Using Perceptual Criteria. *J. Appl. Crystallogr.* **1992**, *25*, 495–503.

(50) Porod, G. *Small Angle X-Ray Scattering*; O., G., Kratky, O., Eds.; Academic Press: London, 1982.

Tables

Table 1. Oligonucleotide sequences of donor labeled hairpins, revelator and targets used.

	Oligonucleotide Sequence (5' → 3')	3' Modification
e13A (hairpin)	ccacgccaaa**cgctgaagggcttcttccttat**ttttggcgtgg	6-carboxyfluorcein
e14A Hairpin	cacctcgaaat**ctgaagggcttttgaactctg**ttttcgaggtg	6-carboxyfluorcein
e13B e13a2 sequence (AJ131467.1)	ataaggaagaagcccttcagcg	-
e14B e13a2 sequence (AJ131466.1)	cagagttcaaaagcccttcag	-
Y Non-complementary	attaccagacatgcgtggtcccaac	-
e13C Revelator for e13A	ccacgccaaa	ROX
e14C Revelator for e14A	cacctcgaaa	Dy-520XL Megastockes

Bold – Recognition portion of the hairpin, Underline – Revelator hybridization region

Table 2. The overall structural parameters estimated from SAXS data. R_g – radius of gyration, D_{max} – maximum size of the particle, V_P – excluded volume of the particle, χ^2 - fit quality of *ab initio* models to experimental data.

Sample	R_g nm	D_{max} nm	V_P nm^3	χ^2
e13A	2.36	8.0	24	1.58
e13B	1.86	7.0	13	0.85
e13C	1.32	5.0	8	0.86
e13AB	5.40	20.0	103	1.85
e13ABC	4.56	18.0	59	1.78
e14A	2.93	12.5	34	1.34
e14B	2.05	9.0	15	0.93
e14C	1.29	5.0	7	0.91
e14AB	5.85	22.5	159	1.31
e14ABC	5.21	20.0	105	1.87
e13A-e14B-e13C	3.95	18.0	65	0.76
e14A-e13B-e14C	3.80	14.0	42	1.29

Figure legends

Figure 1. Schematic representation of the recognition principle used in the developed biosensor. A– Hairpin in the closed conformation, B– Secondary structure disruption due to hybridization to the target sequence, C– Hybridization of acceptor labeled oligonucleotide to exposed hairpin sequence renders a positive FRET signal.

Figure 2. FRET analyses of the two-component molecular beacon towards the sequence e14a2 in different conditions. Top panel: Cartoon representation of the tested conditions. Middle and bottom panel: Emission spectra collected in different scenarios for hairpin e14A. I) Emission spectra of e14A in the absence of e14B, II) Emission spectra of e14A hybridized to e14B, III) Emission spectra of e14A and e14C in the presence of non-complementary target (e14AYC), IV) Emission of spectra e14A and e14C in the presence of e13B (e14A-e13B-e14C), V) Emission of spectra e14A and e14C in the presence of e14B (e14ABC), VI) and VII) Normalized donor emission of e14A in the absence (A) and presence of complementary target (B), C), D) and E) Ratiometric analysis of donor and acceptor channels in different scenarios (negative target, partial complementary target, and fully complementary target, respectively). Data presented as the mean ± standard deviation of three independent assays.

Figure 3. Experimental SAXS patterns for the hairpin towards the e14a2 fusion sequence. (1) e13 hairpin – e14A; (2) e14A in the presence of e14a2 target sequence – e14AB; (3) e14A in the presence of e14a2 target and revelator – e14ABC. The plots display the logarithm of the scattering intensity as a function of momentum transfer. The curves are shifted by one logarithm unit for better visualization. The insert shows the distance distribution functions *P(r)*.

Figure 4. Microscale thermophoresis analysis. Binding curves used to determine the affinity of interaction, black circles – fully complementary target, grey circles – partial complementary target, black squares – acceptor labeled oligonucleotide, Data presented as the mean ± standard deviation of three independent assays.